Nanoscale

Cite this: *Nanoscale*, 2012, **4**, 3466

www.rsc.org/nanoscale

**PAPER**

# Three-dimensional hierarchical flower-like Mg–Al-layered double hydroxides: highly efficient adsorbents for As(V) and Cr(VI) removal†

**Xin-Yao Yu, Tao Luo, Yong Jia, Ren-Xia Xu, Chao Gao, Yong-Xing Zhang, Jin-Huai Liu and Xing-Jiu Huang***

***Received 26th February 2012, Accepted 27th March 2012***
**DOI: 10.1039/c2nr30457k**



3D hierarchical flower-like Mg–Al-layered double hydroxides (Mg–Al-LDHs) were synthesized by a simple solvothermal method in a mixed solution of ethylene glycol (EG) and water. The formation mechanism of the flower-like Mg–Al-LDHs was proposed. After calcination, the flower-like morphology could be completely preserved. With relatively high specific surface areas, Mg–Al-LDHs and calcined Mg–Al-LDHs with 3D hierarchical nanostructures were tested for their application in water purification. When tested as adsorbents in As(V) and Cr(VI) removal, the as-prepared calcined Mg–Al-LDHs showed excellent performance, and the adsorption capacities of calcined Mg–Al-LDHs for As(V) and Cr(VI) were better than those of Mg–Al-LDHs. The adsorption isotherms, kinetics and mechanisms for As(V) and Cr(VI) onto calcined Mg–Al-LDHs were also investigated. The high uptake capability of the as-prepared novel 3D hierarchical calcined Mg–Al-LDHs make it a potentially attractive adsorbent in water purification. Also, this facile strategy may be extended to synthesize other LDHs with 3D hierarchical nanostructures, which may find many other applications due to their novel structural features.

## 1. Introduction

Layered double hydroxides (LDHs), also well known as hydrotalcite-like compounds, and their calcined LDHs (CLDHs) have been used in a wide range of important areas, such as catalysis, photochemistry, biomedical science, electrochemistry, polymerization, environmental application and so on.[1–7] The general formula of LDHs can be expressed as $[M^{II}_{1-x}M^{III}_{x}(OH)_2][A^{n-}_{x/n}]\cdot mH_2O$, where $M^{II}$ and $M^{III}$ are di- and trivalent metal cations in the octahedral positions of brucite-like layers yielding excessive positive charge and $A^{n-}$ represents an *n*-valent anion which balances the positive charges on the layers.[8] After calcination, LDHs are converted to calcined LDHs (CLDHs). CLDHs are able to recover the original layered structures of LDHs, a property known as "memory effect".[8] Large surface area, high anion exchange capacity and good stability are their most interesting properties. Recently, increasing interests have been focused on evaluating the ability of LDHs and CLDHs to remove inorganic contaminants such as oxyanions from aqueous solutions by the process of ion exchange and adsorption.[1,9–12] However, the adsorption capacities of these LDHs and CLDHs are not very high and the adsorption mechanisms were not given.

Considering the fact that the diversity of the morphology of materials has a significant effect on functional diversification and potential applications, considerable efforts have been focused on tuning the morphology and size of nanomaterials in the past decade. Especially, 3D hierarchical nanostructures have attracted much attention due to their unique properties and potential applications.[13–21] It is known that the LDHs materials synthesized by conventional coprecipitation methods usually exhibit stone-like and plate-like morphologies.[8,11,22] The morphological tuning of LDHs is of significant scientific importance as it could influence their electronic, magnetic, optical, catalytic, adsorption properties and so on. Couples of reports on preparation of 3D LDHs spheres have been reported.[23–25] For example, Sasaki *et al.* synthesized Mg–Al-LDH hollow spheres using polystyrene beads as a sacrificial template[23] while Xu *et al.* assembled LDH nanocrystals on carbon nanospheres to fabricate hollow LDH spheres.[24] He and Li synthesized the special spherical aggregate of LDH particles in sodium dodecanesulfonate aqueous solution by hydrothermal treatment.[25] Xu and Gunawan synthesized unusual coral-like LDHs microspheres in an ethylene glycol (EG)–methanol–dodecyl sulfate system.[2] The experimental conditions were too complex as two polar solvents and one surfactant were used and a well-defined 3D hierarchical LDHs morphology cannot be found in their study.[2] Although some 3D LDHs have been fabricated, all of the above works used either hard templates or surfactants. We all know that it is very complicated to remove the hard templates and too many surfactants are known as toxic organic compounds. It is still a great challenge to develop a facile and environmentally friendly

*Research Center for Biomimetic Functional Materials and Sensing Devices, Institute of Intelligent Machines, Chinese Academy of Sciences, Hefei, Anhui 230031, People's Republic of China. E-mail: xingjiuhuang@iim.ac.cn; Fax: +86-551-5592420; Tel: +86-551-5591142*

† Electronic supplementary information (ESI) available. See DOI: 10.1039/c2nr30457k

method for the synthesis of 3D hierarchically structured LDHs with tunable chemical compositions and desirable functions.

A facile and environmentally friendly method for the synthesis of 3D hierarchical Mg–Al-LDHs and calcined Mg–Al-LDHs with higher adsorption capacity for both As(v) and Cr(vi) is still limited in the literature. Herein, we demonstrate the facile synthesis of 3D hierarchical Mg–Al-LDHs *via* an EG-mediated solvothermal method. The unusual 3D hierarchical LDHs can be obtained on a large scale *via* this simple one-pot method. Experimental conditions were varied to investigate the formation mechanism of the 3D hierarchical LDHs. The CLDHs were also obtained *via* calcination. In view of their relatively high specific surface areas, the adsorption performances of LDHs and CLDHs for removing As(v) and Cr(vi) from water were evaluated. The adsorption mechanisms of As(v) and Cr(vi) on LDHs and CLDHs were also proposed.

## 2. Experimental

### Materials

Magnesium nitrate hexahydrate ($Mg(NO_3)_2\cdot 6H_2O$), aluminium nitrate nonahydrate ($Al(NO_3)_3\cdot 9H_2O$), urea, EG, ethanol, nitric acid ($HNO_3$), sodium hydroxide (NaOH), sodium arsenate dodecahydrate ($Na_3AsO_4\cdot 12H_2O$) and potassium dichromate ($K_2Cr_2O_7$) were obtained from Sinopharm Chemical Reagent Co., Ltd., Shanghai, China. As(v) and Cr(vi) stock solution with a concentration of 1000 mg $L^{-1}$ were prepared by dissolving $Na_3AsO_4\cdot 12H_2O$ and $K_2Cr_2O_7$ in double deionized water. All chemicals were of analytical grade and used without further purification.

### Synthesis of 3D hierarchical flower-like Mg–Al-LDHs and calcined Mg–Al-LDHs

In a typical synthesis, $Mg(NO_3)_2\cdot 6H_2O$, $Al(NO_3)_3\cdot 9H_2O$ and urea with a molar ratio of 2 : 1 : 15 were dissolved and stirred in a mixed solvent of EG and $H_2O$ (volume ratio 9 : 1) for 0.5 h at room temperature. Then the homogeneous solutions were transferred into a 60 mL Teflon-lined autoclave and heated at 160 °C for 6 h. After cooling to room temperature naturally, the solid precipitate was collected by centrifugation and washed three times with water and ethanol, respectively. The as-prepared samples were dried at 100 °C for 12 h. The calcined Mg–Al-LDHs were prepared by calcining Mg–Al-LDHs at 500 °C for 3 h and 8 h.

### Adsorption experiments

For the comparison of As(v)/Cr(vi) adsorption performances between LDHs and calcined LDHs, the initial As(v) and Cr(vi) concentrations were 13.64 and 16.67 ppm, respectively, and the adsorbent dose was 0.35 g $L^{-1}$ in a comparison study. For the equilibrium adsorption isotherm study, calcined LDHs with a loading of 0.35 g $L^{-1}$ were added to As(v)/Cr(vi) solutions with different initial concentrations. The pH values of all these As(v) solutions were adjusted to 7.0 ± 0.2, while for Cr(vi) solutions they were 6.5 ± 0.2. In the comparative and adsorption isotherm studies, the adsorption experiments were conducted in a 10 mL polyethylene centrifuge tubes by using the batch technique. These samples were mounted on the shaker for stirring 24 h. The adsorption capacity of the adsorbents for As(v)/Cr(vi) was calculated according to the following equation:

$$q_e = \frac{(C_0 - C_e)V}{m} \quad (1)$$

where $C_0$ and $C_e$ represent the initial and equilibrium As(v)/Cr(vi) concentrations (mg $L^{-1}$), respectively. $V$ is the volume of the As(v)/Cr(vi) solution (mL), and $m$ is the amount of adsorbent (mg).

In the kinetic study of As(v)/Cr(vi) adsorption on calcined LDHs samples, the initial As(v) and Cr(vi) concentrations were 3.534 and 3.583 ppm, respectively. The experiments were carried out using a 250 mL conical flask containing 100 mL of an As(v)/Cr(vi) solution, and the adsorbent dose was 0.2 g $L^{-1}$ in the kinetics study. The pH values of all the As(v)/Cr(vi) solutions were adjusted by using $HNO_3$ and NaOH as that in adsorption isotherm study. And these samples were placed on a shaker for stirring. At predetermined time intervals, stirring was interrupted while 6 mL of supernatant solutions were pipetted and centrifuged for the determination of the remaining arsenic concentrations.

All the adsorption experiments were carried out at room temperature (298 ± 2 K). All the experimental data were the average of triplicate determinations. The relative errors of the data were about 5%.

### Characterization

Scanning electron microscopy (SEM) images were obtained with a FEI Quanta 200 FEG field emission scanning electron microscope. Transmission electron microscopy (TEM), high-resolution TEM (HRTEM) and energy-dispersive spectrometer analysis (EDS) analyses were performed using a JEM-2010 microscope equipped with Oxford INCA EDS operated at 200 kV accelerating voltage (Quantitative method: Cliff Lorimer thin ratio section). X-Ray diffraction (XRD) was performed on a D/MaxIIIA X-ray diffractometer (Rigaku Co., Japan), using Cu Kα ($\lambda_{K\alpha 1}$ = 1.5418 Å) as the radiation source. Thermogravimetric/derivative thermogravimetric (TG/DTG) analysis was performed on a SDT-Q600 DTG-TGA instrument. The nitrogen adsorption and desorption isotherms at 77 K were measured with a Micromeritics ASAP 2020 M analyzer. The Brunauer, Emmett, and Teller (BET) equation was used to obtain the specific surface areas. The Fourier transform infrared (FT-IR) spectra of the obtained samples were recorded with a NEXUS-870 FT-IR spectrometer in the range of 4000–400 $cm^{-1}$. The As(v) and Cr(vi) concentrations were determined in the liquid phase using inductively coupled plasma atomic emission spectrometry (ICP-AES, Jarrell-Ash model ICAP 9000).

## 3. Results and discussion

Fig. 1a–c showed the morphological features of the sample which was synthesized in the mixture of water and EG of 1 : 9 volumetric ratio at 160 °C for 6 h. Fig. 1a and b displayed the typical SEM images with different magnifications of the as-synthesized Mg–Al-LDHs. Distinct from the conventional stone-like aggregates, uniform 3D flower-like Mg–Al-LDHs spheres comprised

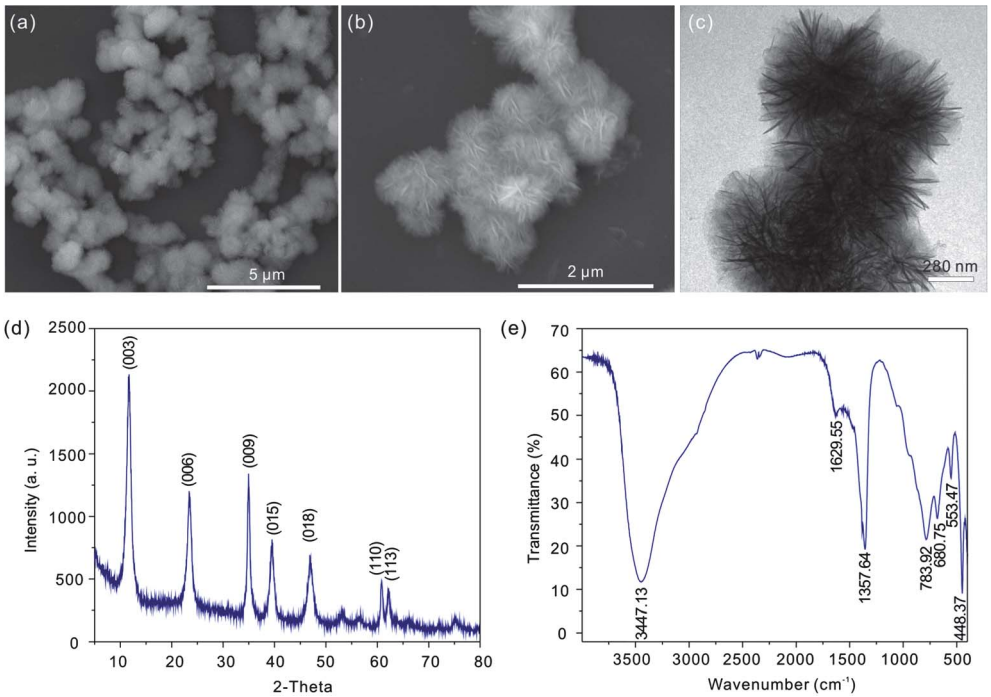


**Fig. 1** (a) Low-magnification SEM image; (b) high-magnification SEM image; (c) TEM image; (d) XRD pattern and (e) FTIR spectra of the as-obtained Mg–Al-LDHs. Water/EG = 1 : 9, $Mg^{2+}$ : $Al^{3+}$ : urea = 2 : 1 : 15, $T$ = 160 °C and $t$ = 6 h.

of self-organized nanoplates with a diameter about 0.5–1 μm can be observed in Fig. 1b. This structure was also confirmed by the TEM image shown in Fig. 1c. The thin, smooth and curved nanoplates can be clearly observed. A series of other measurements were also used to investigate the as-prepared Mg–Al-LDHs. The XRD pattern of the as-prepared sample shown in Fig. 1d can be indexed to a rhombohedral $Mg_{0.67}Al_{0.33}(OH)_2(CO_3)_{0.165}\cdot 0.48H_2O$ (JCPDS file No. 89-5434). It presented the characteristic reflections of a typical hydrotalcite-like material with a series of symmetric (0 0 $l$) peaks at lower 2$\theta$ values corresponding to successive orders of basal spacing and relatively weak non-basal reflections at higher 2$\theta$ values. The interlayer $d$-spacing of characteristic (0 0 3) planes ($d_{003}$) at 2$\theta$ = 11.67° was found to be 0.758 nm. The chemical composition of the as-obtained Mg–Al-LDHs was also characterized by EDS (Fig. S1, ESI†). Peaks of the elements Mg and Al were detected in the EDS pattern and the molar ratio was about 2 : 1 which was in agreement with the XRD result. The FTIR spectrum of the as-obtained Mg–Al-LDHs was given in Fig. 1e. The adsorption peaks in the range of 500–800 $cm^{-1}$ were associated with M–O, O–M–O, and M–O–M lattice vibrations (M = Mg and Al). The strong peak at 1357.64 $cm^{-1}$ was due to the vibration mode of $CO_3^{2-}$ ions in the interlayer of Mg–Al-LDHs, and the band at 1629.55 $cm^{-1}$ belonged to the hydroxyl deformation mode of the water molecules in the interlayer. The strong peak at 3447.13 $cm^{-1}$ was attributed to the stretching modes of the OH groups associated with the interlayer water molecules and hydrogen bonding. The FTIR spectrum further confirmed the presence of intercalated $CO_3^{2-}$, OH groups and water molecules.

The morphologies and phase purity of the as-synthesized samples were mainly affected by the following experimental conditions, such as the ratio of $H_2O$ to EG, amount of urea used, ratio of $Mg^{2+}$ to $Al^{3+}$ and the reaction temperature. Firstly, we systematically studied the effect of the volume ratio of $H_2O$ to EG on the structure and morphology of the resultant products. In these experiments, the molar ratio of $Mg^{2+}$ : $Al^{3+}$ : urea, reaction temperature and reaction time was fixed at 2 : 1 : 9, 160 °C and 6 h, respectively. When different volume ratios of $H_2O$/EG were used in the reaction system, the corresponding morphology variations of the products were shown in Fig. S2a in the ESI.† As can be seen from Fig. S2a in the ESI, without the addition of EG, two kinds of morphology, fiber-like and plate-like products can be obtained. The further XRD (Fig. S3a, ESI) and FTIR (Fig. S4a, ESI)† measurements confirmed that this sample was not the Mg–Al-LDHs. We noticed that with the addition of EG ($H_2O$ : EG = 4 : 1), the fiber-like samples decreased. When the ratio of $H_2O$ to EG decreased to 1 : 1 only plate-like samples were observed. However, we cannot get pure Mg–Al-LDHs at both of these two $H_2O$ : EG ratios as can be seen from XRD (Fig. S3b and c, ESI) and FTIR (Fig. S4b and c, ESI) measurements† which showed that there were some peaks and bands not belonging to Mg–Al-LDHs. As the ratio of $H_2O$ to EG decreased to 1 : 4, Mg–Al-LDHs with pure phase were obtained (Fig. S3d and S4d, ESI).† From the TEM image (inset of Fig. S2d, ES) we can see that this sample was composed of plate-like fragments. When EG occupied 90% of the volume, 3D hierarchically flower-like products appeared (Fig. S2d, ESI) although this sample was not pure Mg–Al-LDHs confirmed by XRD and FTIR measurements (Fig. S3e and S4e, ESI). In pure EG, from Fig. S2f in the ESI we can see that well dispersed 3D structures cannot be obtained in this condition. It was also difficult to identify the phase of this sample (Fig. S3f, ESI). And from the FTIR measurement (Fig. S4f, ESI), the band of $CO_3^{2-}$ ions cannot be found confirming that this sample was not

 

Mg–Al-LDHs. It was clear that the amount of EG played an important role for the phase purity and shapes of the resulted samples. In order to get pure Mg–Al-LDHs with well-defined 3D hierarchical nanostructures, the ratio of $H_2O$ to EG was fixed at 1 : 9 and other experimental conditions were varied.

Secondly, it is worthwhile to mention that the amount of urea used had strong effects on the formation of pure Mg–Al-LDHs and well-defined 3D hierarchical nanostructures. In this section, the ratio of $Mg^{2+}$ to $Al^{3+}$ was fixed at 2 : 1 and the ratio of EG/$H_2O$ was fixed 9 : 1. Reaction temperature and time were not changed. Fig. S5 in the ESI† shows the SEM images of the samples obtained when the ratio of $Mg^{2+}$ : $Al^{3+}$ : urea was 2 : 1 : 6 and 2 : 1 : 18, respectively. Fig. S6 in the ESI† showed the XRD patterns of these two samples. Combined with the XRD results of the other two samples synthesized when the ratio of $Mg^{2+}$ : $Al^{3+}$ : urea was 2 : 1 : 15 (Fig. 1d) and 2 : 1 : 9 (Fig. S3e, ESI), we can conclude that with the increase of urea the phase of the products became pure. When the ratio of $Mg^{2+}$ : $Al^{3+}$ : urea was 2 : 1 : 15 a well-defined 3D flower-like Mg–Al-LDHs with pure phase could be obtained. With the further increase of urea (2 : 1 : 18) the 3D nanostructures tended to collapse (Fig. S5b, ESI). Therefore, the amount of urea added was very critical in this synthesis method. It is known that urea in aqueous solution can provide steadily $OH^-$ ion by hydrolysis and release $CO_2$ at the same time.[15] On the one hand, the proper amount of urea was very helpful to obtain pure Mg–Al-LDHs. On the other hand, an excessive amount of urea would release $CO_2$ vigorously which may lead to the collapse of the 3D nanostructures.

The effects of the ratio of $Mg^{2+}$ to $Al^{3+}$ on the morphology and the phase purity of Mg–Al-LDHs were also investigated. In this section, the ratio of $Mg^{2+}$ to $Al^{3+}$ was changed. Fig. S7a and b in the ESI† showed the SEM images of samples synthesized when the ratio of $Mg^{2+}$ to $Al^{3+}$ was 3 : 1 and 4 : 1, respectively. We can see that these two samples had similar morphology: stacks of irregular stone-like spheres. In addition, the 3D hierarchical nanostructures did not appear at these two $Mg^{2+}/Al^{3+}$ ratios. Further XRD (Fig. S8a and b, ESI) and FTIR (Fig. S8c and d, ESI)† measurements revealed that these two samples were not pure Mg–Al-LDHs.

Reaction temperature is critical in hydrothermal/solvothermal experiments. We also studied the reaction temperature effects. Fig. S9 in the ESI† gave the SEM and TEM images of the samples prepared at temperature of 140 °C, 180 °C and 200 °C, respectively. As can be seen from Fig. S9a and b in the ESI and the inset TEM images of Fig. S9a and b, 3D hierarchical nanostructures also appeared at the reaction temperature of 140 °C and 180 °C. However, the XRD patterns (Fig. S10a and b, ESI†) revealed that these two samples were not pure Mg–Al-LDHs. When the reaction temperature was increased to 200 °C, the 3D hierarchical nanostructures disappeared and microcrystals were observed. XRD results (Fig. S10c, ESI)† showed that this sample was not pure Mg–Al-LDHs either.

In order to understand the formation process of the 3D hierarchical nanostructures, time-dependent experiments were performed. Fig. S11 in the ESI† showed the SEM images of the samples obtained at different time intervals. At the early stages (20 min), the samples were composed of nanoparticles (Fig. S11a, ESI). After the hydrothermal treatment for 40 min, some irregular 3D hierarchical structures assembled with nanoplates appeared (Fig. S11b, ESI). When the reaction time was extended to 2 h, uniform 3D hierarchical nanostructured spheres with larger size could be clearly observed as shown in Fig. S11c in the ESI. The image indicated that nanoflakes began to form on the outside of these spheres. On further prolonging the reaction time (Fig. 1b) to 6 h, all the samples collected were well-defined 3D flower-like nanostructures which were composed of nanoplates from the inside to the outside. The morphological evolution with time clearly illustrated that the sample formed according to a stepwise growth mechanism. On the basis of the above characterization results, a possible formation mechanism of the 3D hierarchically flower-like Mg–Al-LDHs nanostructures is illustrated in Fig. 2. In our experiments, both urea and EG played essential roles in the morphological transformation. In conventional precipitation methods, the precipitation of LDHs occurs immediately upon the mixing of metal ions and alkali, which usually results in stone-like products. In contrast, uniform nanocrystals were obtained upon nucleation and crystallization in our experiments due to the following reasons. Urea provided a steady $OH^-$ ion source through gradual hydrolysis which prevented fast precipitation. In this growth stage, $Mg^{2+}$ and $Al^{3+}$ ions coprecipitated and formed Mg–Al-LDHs crystal nuclei, which provided the necessary heterogeneous nucleation sites. EG as complexing agent could coordinate with $Mg^{2+}$ and $Al^{3+}$ ions, which reduced the nucleation and growth rate of the LDHs and prohibited them developing into bigger ones during the crystallization process. As a greater volume ratio of EG existed in this solvent system, it formed vesicles which served as template to induce LDH growth to form curved or contorted LDH sheets. In the following secondary growth stage, in order to minimize their surface energy, release the strong stress, and then under external conditions such as electrostatic and dipolar fields associated with hydrogen bonds, hydrophobic interactions and van der Waals forces, curved or contorted nanosheets self-assembled into irregular 3D nanostructures in the next growth stage.[26–28] At a sufficiently high temperature (160 °C) and 2 hours' aging time, some irregular 3D nanostructured LDH aggregates merged together into uniform 3D hierarchical nanospheres. Sheet-curved LDHs grew deeper within the spheres with further aging, resulting in stable spherical 3D flower-like aggregation. Similar

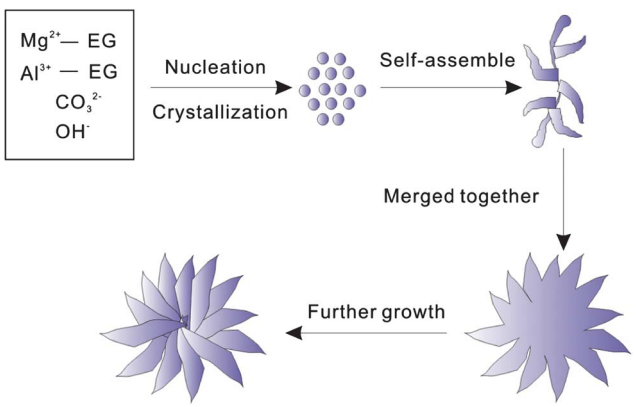


**Fig. 2** Schematic illustration of the morphological evolution process of the 3D hierarchical flower-like Mg–Al-LDHs.

results have also been reported by He and Li.[25] In Xu *et al.* and He *et al.*'s studies, sodium dodecanesulfonate was used both as interlayer anions and the morphology-controlling agent for the formation of LDH sheets.[2,25,29] Sun and Hu used CATB to fabricate 3D micro–nano structures.[30] CTAB in aqueous solutions might aggregate to form spherical or cylinder micelles and the positively charged CTAB head groups may attract negatively charged $OH^-$.[30] However, the CTAB did not get into the interlayer of LDHs.[30] All of the above studies used the charged properties of surfactants to control the morphology of the products. However, in this study, no surfactants were used and EG coordinated with $Mg^{2+}$ and $Al^{3+}$. LDH crystals grow along EG vesicle interfaces and consequently, the curved and contorted LDH nanoplates are assembled into aggregates. EG was not incorporated as an interlayer molecule, which has been proved by FT-IR study (Fig. 1e).

Thermal analysis experiments were employed to characterize further the thermal stability of the as-prepared 3D hierarchical nanostructures. The TG and DTA results were presented in Fig. 3. Generally, four weight loss steps are observed in the thermal evolution of LDHs: (i) desorption of physically adsorbed water; (ii) removal of the interlayer structural water; (iii) dehydroxylation of the brucite-like layers; and (iv) decomposition of the interlayer anions. The first two steps may overlap in the temperature range from 30 to 200 °C and the latter two steps may also overlap at higher temperatures.[31,32] For the thermal decomposition of the 3D Mg–Al-LDHs nanostructures studied here, three distinct weight loss steps were observed in both TG and DTA curves. The first step from room temperature to approximately 85 °C corresponded to the removal of the surface adsorbed water. The second weight loss step from 85 °C to approximately 200 °C was due to removal of the interlayer water molecules. The third weight loss step in the temperature range from 250 to 450 °C was due to the dehydroxylation of the brucite-like layers accompanied by the decomposition of interlayer carbonate anions.

The calcination temperature and time were two key parameters to be controlled in the calcination process. The calcination temperature must be high enough to eliminate most of the $CO_3^{2-}$ ions and low enough to permit the layer reconstruction, since too high a temperature may hinder or make difficult the reconstruction of LDHs. In addition, higher calcination temperature and quicker heating rate may lead to the collapse of the spherical morphology. So in this study the chosen temperature for calcination of the LDHs was 500 °C and the heating rate was 1 °C $min^{-1}$, and two calcination times – 3 h and 8 h – were used. These two calcined products were assigned as CLDHs-3h and CLDHs-8h, respectively. Fig. 4a and b gives the morphological features of the calcined samples. We can see that the morphology of the Mg–Al-LDHs did not change even after 8 h of calcination, which illustrated the good thermal stability of this 3D hierarchical nanostructure. The inset TEM images of Fig. 4a and b also testified the integrity of the calcined products. Fig. 4c shows the FTIR spectra of CLDHs-3h and CLDHs-8h. Compared to LDHs, the peak intensity of $CO_3^{2-}$ ions at 1357.64 $cm^{-1}$ changed little for CLDHs-3h, while the intensity of this peak for CLDHs-8h became relatively weaker. This indicated that more $CO_3^{2-}$ ions in the interlayer were removed after 8 h of calcination. The XRD patterns of CLDHs-3h and CLDHs-8h were shown in Fig. 4d. As can be seen from Fig. 4d the XRD pattern still had the characteristics of LDHs after 3 h of calcination indicating that the $CO_3^{2-}$ ions were not effectively removed and only a little of the layered hydrotalcite-like structure was destroyed in this condition. After the sample was calcined for 8 h, the layered hydrotalcite-like structure disappeared, leading to the formation of a mixed magnesium aluminium oxide. Only the peaks of magnesium oxide could be found in the pattern, which may be the result of aluminium getting into the lattice of magnesium oxide during calcination.

Fig. 5 presents the $N_2$ adsorption–desorption isotherms of LDHs, CLDHs-3h and CLDHs-8h. All of the isotherms can be categorized as type IV. The BET surface area of LDHs was 118.17 $m^2\ g^{-1}$. After calcination the BET surface area of CLDHs increased to 219.54 $m^2\ g^{-1}$ (CLDHs-3h) and 225.43 $m^2\ g^{-1}$ (CLDHs-8h).

As(v) and Cr(vi) are considered primary highly toxic micropollutants in water resources and their efficient removal is considered to be of great importance. To investigate the potential

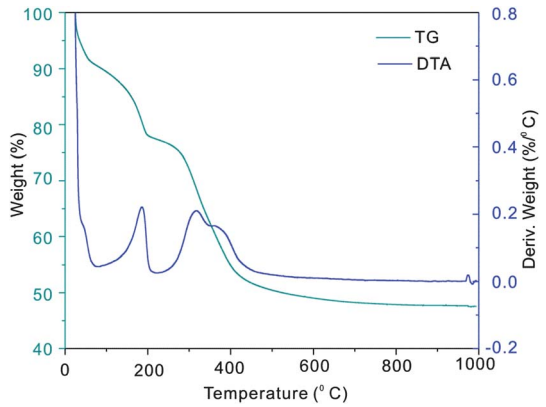


**Fig. 3** TG-DTA curves of as-obtained Mg–Al-LDHs.

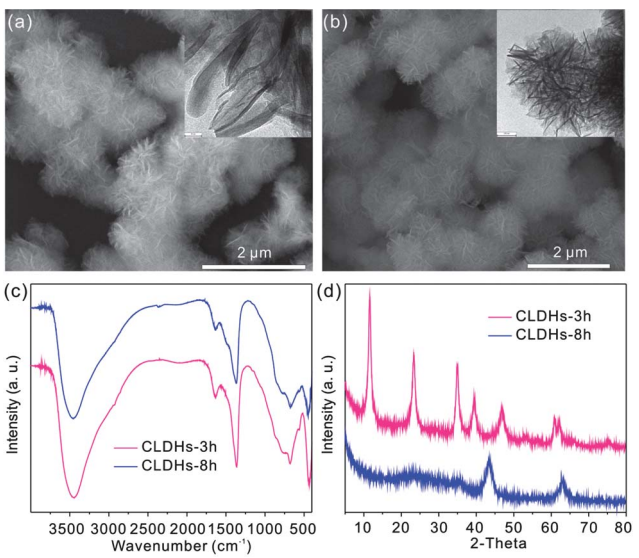


**Fig. 4** SEM images of CLDHs at different times: (a) 3 h and (b) 8 h; (c) FTIR spectra and (d) XRD patterns of CLDHs.

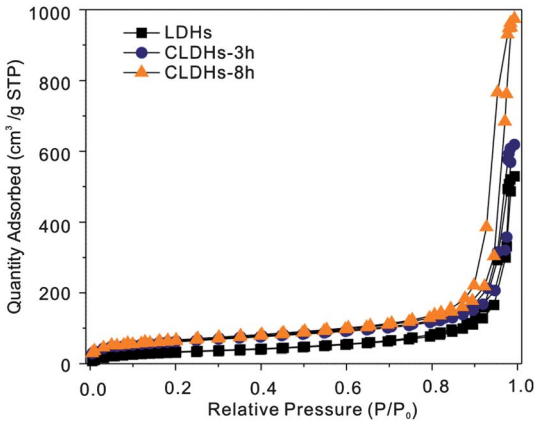


**Fig. 5** Nitrogen adsorption and desorption isotherms of LDHs and CLDHs.

application of the synthesized 3D hierarchical LDHs and CLDHs in water purification, the adsorption performance of LDHs and CLDHs for As(v) and Cr(vi) were tested. Fig. S12 in the ESI† showed the As(v)/Cr(vi) adsorption performance of LDHs and CLDHs samples at an initial As(v)/Cr(vi) concentration of 13.64 ppm/16.67 ppm. For both As(v) and Cr(vi) adsorption, CLDHs-3h and CLDHs-8h both showed a higher adsorption capacity than LDHs, and CLDHs-8h had a higher adsorption capacity than CLDHs-3h. Uncalcined LDHs can remove anions from solution by two different mechanisms: (i) adsorption of anions on the external surface as the pH of zero point of charge of LDHs is up to 12,[1] and (ii) intercalation by anion exchange. When $CO_3^{2-}$ ions are present as the interlayer anion, the anion exchange becomes very difficult due to its strong electrostatic interaction with the layers. So in this study the main adsorption mechanism for As(v)/Cr(vi) adsorption onto LDHs was adsorption of anions onto their external surface. After 3 h of calcination, due to the removal of some $CO_3^{2-}$ ions and the increase of BET surface area the adsorption capacity of CLDHs-3h for As(v) and Cr(vi) increased. For the CLDHs, the adsorption mechanism may involve the rehydration of mixed metal oxides and concurrent intercalation of As(v)/Cr(vi) into the interlayer to reconstruct the LDHs (in the following adsorption mechanisms study we will give the evidence). So, the differences in adsorption capacity between LDHs and CLDHs may be linked to three main reasons: (i) the increase of specific surface area of the calcined products; (ii) fewer $CO_3^{2-}$ ions exist in the interlayer of the CLDHs than in the LDHs; and (iii) the different adsorption mechanisms between LDHs and CLDHs.

The adsorption capacities of CLDHs for As(v) and Cr(vi) were evaluated using the equilibrium adsorption isotherm by varying the initial anion concentrations. Fig. 6a showed the adsorption isotherms of As(v)/Cr(vi) onto CLDHs-3h and CLDHs-8h at room temperature. From Fig. 6a we can see that the adsorption capacity of CLDHs-8h for both As(v) and Cr(vi) was higher than that of CLDHs-3h. This may be due to the higher specific surface area of CLDHs-8h and that less carbonate ions remained in its interlayer. Two empirical equations, the Langmuir and Freundlich isotherm models, were used to analyze the experimental data. The mathematical expressions of the Langmuir isotherm and the Freundlich isotherms model are[33,34]

$$\frac{C_e}{q_e} = \frac{1}{q_m K_L} + \frac{C_e}{q_m} \quad (2)$$

$$\ln q_e = \frac{1}{n} \ln\ C_e + \ln K_F \quad (3)$$

where $q_m$ and $K_L$ are Langmuir constants, representing the maximum adsorption capacity of adsorbents (mg $g^{-1}$) and the energy of adsorption, respectively. $K_F$ and $n$ are Freundlich constants related to adsorption capacity and adsorption intensity, respectively.

For the Langmuir isotherm model, the values of $q_m$ and $K_L$ can be calculated from the slope and intercept of plots of $C_e/q_e$ *versus* $C_e$. And for the Freundlich isotherm model, the values of $n$ and $K_F$ can be obtained by a plot of ln $q_e$ against ln $C_e$. The linearized Langmuir isotherms (Fig. 6b) and Freundlich isotherms (Fig. S13, ESI†) of As(v) and Cr(vi) onto CLDHs are also shown. The parameters of the Langmuir and Freundlich models were calculated and listed in Table S1 in the ESI.† The maximum capacities of CLDHs-3h and CLDHs-8h for As(v)/Cr(vi) were determined at 92.51/65.32 mg $g^{-1}$ and 216.45/188.32 mg $g^{-1}$, respectively. From the correlation coefficients, it can be seen that the adsorption data for As(v) and Cr(vi) fit the Langmuir isotherm model better than the Freundlich isotherm model. In addition, the maximum adsorption capacity of both CLDHs-3h and CLDH-8 h for As(v) were better than that of Cr(v). Further work is underway to investigate the reason for this point.

To assess the As(v)/Cr(vi) removal performance of CLDHs samples, the adsorption capacity of the CLDHs samples for As(v)/Cr(vi) was compared with other CLDHs and 3D hierarchical metal oxide nanostructures (Table 1). Table 1 indicated that the adsorption capacities of CLDHs samples for both As(v) and Cr(vi) in this study were higher than those of the other CLDHs and 3D hierarchical metal oxide nanostructures. For instance, the adsorption capacities of the γ-$Fe_3O_4$ flower for As(v) and Cr(vi) were just 4.75 and 3.86 mg $g^{-1}$, while for CLDHs in this study the adsorption capacities for As(v) and Cr(vi) were 216.45 and 188.32 mg $g^{-1}$ which were about 46 and 49 times that of the γ-$Fe_3O_4$ flower. The high adsorption capacity was due to the higher specific area, the novel 3D hierarchical nanostructures and different anion uptake mechanisms. More importantly, most results reported in the literature were obtained at low pH values for As(v) and Cr(vi), thus those good removal performances may not be realized at normal pH values in practical water purification. While in this study the removal capacity values of the 3D hierarchical CLDHs were measured under neutral pH values. In addition, the calcined LDHs samples can be regenerated by rinsing with 0.01 M $Na_2CO_3$ solution. More than 90% As(v) and Cr(vi) can be desorbed from the calcined LDH nanostructures. After the second round of calcination, the calcined product can be reused to adsorb As(v) and Cr(vi). In particular, after 5 cycles of reuse, the adsorption capacity of the calcined LDHs nanostructures is still maintained at 80% that of the fresh calcined 3D Mg–Al-LDHs. We also investigated the leaching of Mg(ii) and Al(iii) during the adsorption experiments. In the test time range (0–24 h), the leaching of Mg(ii) and Al(iii) after adsorption of As(v) and Cr(vi) in the concentration range of 0–400 ppm was below 8 and 1.5 ppm, respectively. These

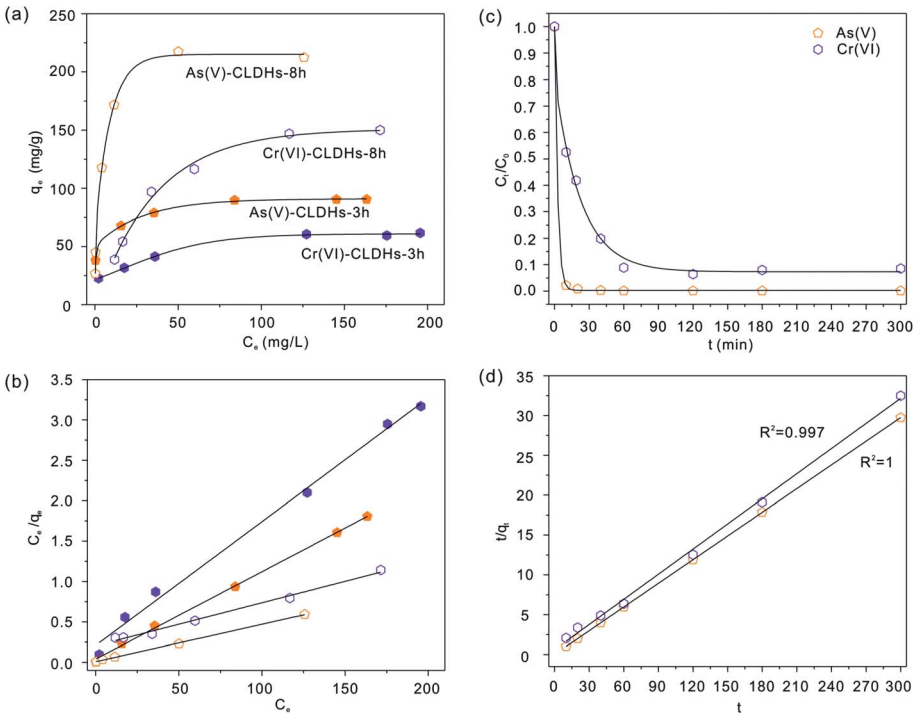


**Fig. 6** (a) Adsorption isotherms and (b) linearized Langmuir isotherms of As(v) and Cr(vi) onto CLDHs; (c) effects of contact time on the adsorption of As(v) and Cr(vi) onto CLDHs-8h; (d) pseudo-second-order kinetic plots for the adsorption of As(v) and Cr(vi) onto CLDHs-8h.

concentrations pose no harm to the human body. We believe that the 3D hierarchical CLDHs nanostructures reported here will have potential practical applications in the purification of water.

The kinetics of adsorption, which describes the solute uptake rate governing the residence time of the adsorption reaction, is one of the most important characteristics that define the efficiency of adsorption. The kinetics of As(v) and Cr(vi) adsorption onto CLDHs-8h were shown in Fig. 6c. It was clear from Fig. 6c that the adsorption rates of As(v) and Cr(vi) were rather fast. In such experimental conditions, most As(v) and Cr(vi) could be removed after 2 h. The above adsorption kinetic experimental data can be best fitted into a pseudo-second-order rate kinetic model. The pseudo-second-order model is presented as follows[33,35]

$$\frac{t}{q_t} = \frac{1}{k_2 q_e^2} + \frac{1}{q_e} t \qquad (4)$$

where $q_e$ and $q_t$ are the amount of As(v)/Cr(vi) adsorbed at equilibrium and at time $t$, respectively. $k_2$ is the rate constant of the pseudo-second-order model of adsorption (g mg$^{-1}$ min$^{-1}$). For the pseudo-second-order model, the values of $k_2$ and $q_e$ can be obtained by a plot of $t/q_t$ against $t$. The pseudo-second-order kinetics plots for the adsorption of As(v) and Cr(vi) onto CLDHs-8h samples were shown in Fig. 6d. Fig. 6d demonstrated that the experimental data could be well fitted with the linear form of the pseudo-second-order model. The correlation coefficient values for the pseudo-second-order model were all above 0.99 (Table S2, ESI†), suggesting that the pseudo-second-order model best represented the adsorption kinetics in our adsorbent systems.

CLDHs-8h after adsorption of As(v) and Cr(vi) were characterized by FTIR (Fig. 7a) and XRD (Fig. 7b) measurements. Compared with LDHs, after interaction with water containing As(v) and Cr(vi), a new band at 846 and 880 cm$^{-1}$ for As(v) and Cr(vi) appeared,[36–38] respectively, indicating that the reconstruction of the layered structure took place with the incorporation of these anions. Fig. 7b gave the XRD patterns of CLDHs-8h after adsorption of As(v) and Cr(vi). Reconstruction of the layered structure was observed to take place after As(v) and Cr(vi) adsorption from the XRD curves. The basal spacing,

**Table 1** Adsorption capacity comparisons of 3D hierarchical CLDHs-8h in this study with other adsorbents for removal of As(v) and Cr(vi)

| | Adsorption capacity/mg g$^{-1}$ | | |
|---|---|---|---|
| Adsorbents | As(v) | Cr(vi) | Reference |
| 3D hierarchical calcined Mg–Al-LDHs | 216.45 | 188.32 | This study |
| Stone-like calcined Mg–Al-LDHs (1) | 99.6 | | 38 |
| Stone-like calcined Mg–Al-LDHs (2) | | 128 | 36 |
| $CeO_2$ flower | 6.7 | 5.8 | 14 |
| $\gamma$-$Fe_2O_3$ flower | 4.75 | 3.86 | 15 |

 

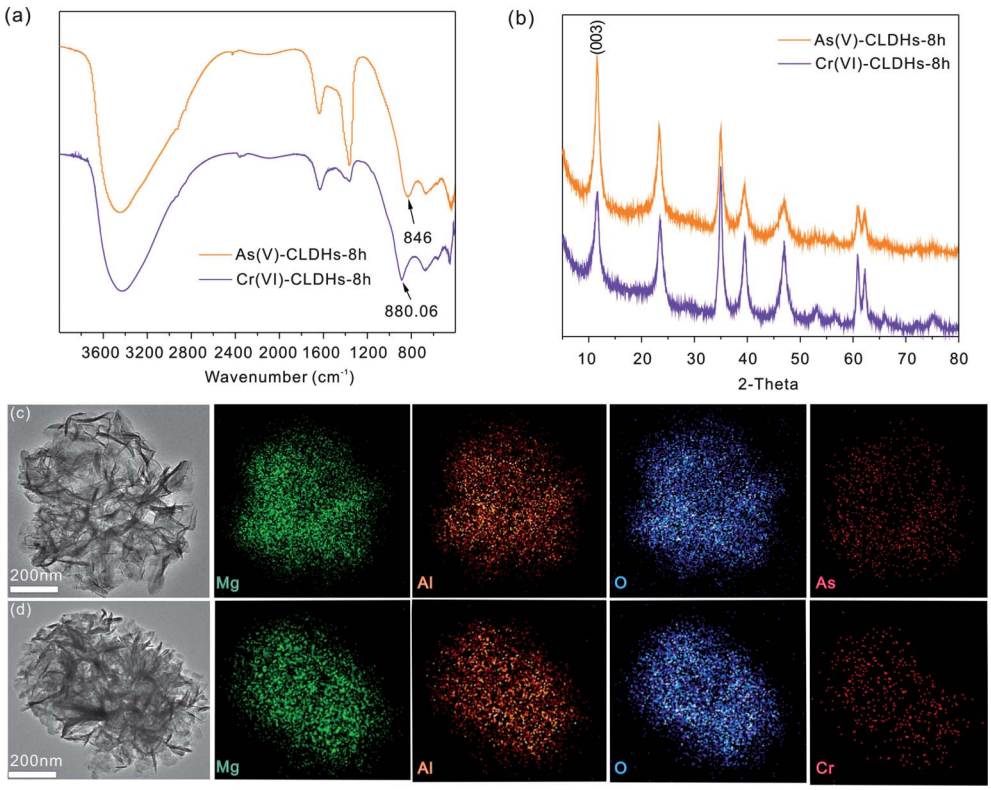


**Fig. 7** (a) FTIR spectra and (b) XRD patterns of CLDHs-8h after adsorption of As(v) and Cr(vi); elemental mapping of CLDHs-8h after adsorption of (c) As(v) and (d) Cr(vi).

$d_{003}$, of CLDHs-8h after adsorption of As(v) and Cr(vi) was 0.768 and 0.762 nm, both of which were larger than that of LDHs (0.758 nm). This also evidenced the entering of As(v) and Cr(vi) into the interlayer of reconstructed LDHs.

For investigation of the element distribution of CLDH-8 h after adsorption of As(v) and Cr(vi), the elemental mapping of Mg, Al, O, As and Cr were elaborated, as shown in Fig. 7c and d. We can see that the distribution of As and Cr was similar to that of Mg, Al and O in the samples, which supported the evidence of As and Cr entering into the layered structure from another point of view.

Based on the above results, a mechanism of uptake of As(v) and Cr(vi) by CLDHs-8h was illustrated in Fig. 8. When the LDHs was calcined at 500 °C for 8 h, dehydroxylation and interlayer carbonate decomposition occured, water and carbon dioxide were released, and the layered structure collapsed. The nanocrystals transformed to mixed magnesium aluminium oxides. In a neutral pH environment, the main species for As(v) and Cr(vi) were $HAsO_4^{2-}$ and $HCrO_4^-$, respectively. After CLDHs reconstruction in a solution containing As(v) or Cr(vi), with the intercalation of $HAsO_4^{2-}$ or $HCrO_4^-$ and $CO_3^{2-}$/$HCO_3^-$/$OH^-$ in water into the layered host structure, the LDH structure reconstructed. The toxic As(v) and Cr(vi) can be effectively removed in this way.

## 4. Conclusions

In summary, we have synthesized hierarchical Mg–Al-LDHs with uniform, self-assembled and 3D flower-like nanostructures by an ethylene glycol-mediated solvothermal method. It has been found that the experimental conditions, especially the ratio of ethylene glycol to water, played a key role in obtaining pure-phase Mg–Al-LDHs with 3D hierarchical nanostructures. A stepwise growth mechanism for 3D hierarchical Mg–Al-LDHs

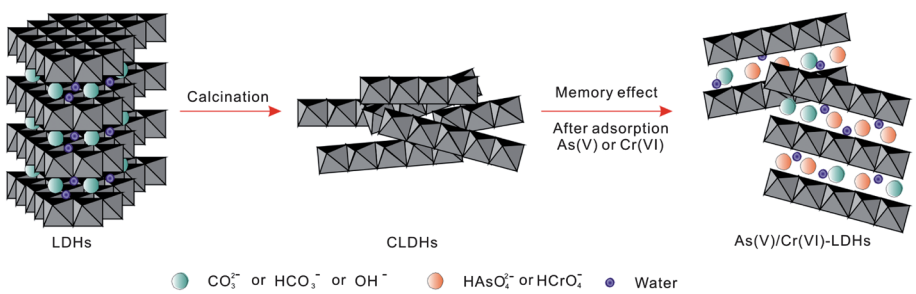


**Fig. 8** A proposed mechanism for the adsorption of As(v) and Cr(vi) onto CLDHs.

was proposed. After converting Mg–Al-LDHs into calcined Mg–Al-LDHs, the obtained calcined products with high surface areas showed no substantial morphological alterations. When tested as adsorbent materials in water purification, calcined Mg–Al-LDHs showed higher performance than Mg–Al-LDHs for As(v) and Cr(vi) removal. The maximum adsorption capacities of the calcined Mg–Al-LDHs thermally treated for 8 h for As(v) and Cr(vi) were 216.45 and 188.32 mg $g^{-1}$, which were better than most reported calcined Mg–Al-LDHs with stone-like morphology and other 3D hierarchical metal oxides. The adsorption rates of As(v) and Cr(vi) onto calcined Mg–Al-LDHs were rather fast. The underlying adsorption kinetics followed the pseudo-second-order model. The XRD, FTIR and elemental mapping measurements evidenced the entering of As(v) and Cr(vi) into the interlayer of reconstructed LDHs. Owing to their novel 3D hierarchical nanostructures and high surface areas, calcined Mg–Al-LDHs are potentially applicable in water purification.

## Acknowledgements

This work was supported by the One Hundred Person Project of the Chinese Academy of Sciences, China, the National Key Scientific Program-Nanoscience and Nanotechnology (no. 2011CB933700), National Natural Science Foundation of China (Grant no. 21103198) and the China Postdoctoral Science Foundation (no. 20110490386 and 2011M501073).

## References

1 T. T. Lim, K. H. Goh and Z. Dong, *Water Res.*, 2008, **42**, 2943–1368.
2 P. Gunawan and R. Xu, *J. Mater. Chem.*, 2008, **18**, 2112–2120.
3 M. S. Yang, J. F. Liu, Z. Chang, G. R. Williams, D. O'Hare, X. H. Zheng, X. M. Sun and X. Duan, *J. Mater. Chem.*, 2011, **21**, 14741–14746.
4 Y. F. Xu, Y. C. Dai, J. Z. Zhou, Z. P. Xu, G. R. Qian and G. Q. M. Lu, *J. Mater. Chem.*, 2010, **20**, 4684–4691.
5 M. C. Lin, F. T. Chang and J. Y. Uan, *J. Mater. Chem.*, 2010, **20**, 6524–6530.
6 R. Z. Ma, Z. P. Liu, L. Li, N. Iyi and T. Sasaki, *J. Mater. Chem.*, 2006, **16**, 3809–3813.
7 C. P. Chen, P. Gunawan and R. Xu, *J. Mater. Chem.*, 2011, **21**, 1218–1225.
8 F. Cavani, F. Trifiro and A. Vaccari, *Catal. Today*, 1991, **11**, 173–301.
9 X. Duan, L. A. Lv, J. He, M. Wei and D. G. Evans, *Water Res.*, 2006, **40**, 2629–743.
10 S. Komarneni, K. Grover and H. Katsuki, *Water Res.*, 2009, **43**, 3884–3890.
11 L. Yang, M. Dadwhal, Z. Shahrivari, M. Ostwal, P. K. T. Liu, M. Sahimi and T. T. Tsotsis, *Ind. Eng. Chem. Res.*, 2006, **45**, 4742–4751.
12 Q. H. Zhang, Y. Zhi, Y. G. Li and H. Z. Wang, *Langmuir*, 2010, **26**, 15546–15553.
13 J. B. Li, J. B. Fei, Y. Cui, J. Zhao, L. Gao and Y. Yang, *J. Mater. Chem.*, 2011, **21**, 11742–11746.
14 L. S. Zhong, J. S. Hu, A. M. Cao, Q. Liu, W. G. Song and L. J. Wan, *Chem. Mater.*, 2007, **19**, 1648–1655.
15 L. S. Zhong, J. S. Hu, H. P. Liang, A. M. Cao, W. G. Song and L. J. Wan, *Adv. Mater.*, 2006, **18**, 2426–2431.
16 S. H. Wu, X. H. Liu, J. Zhang, L. W. Wang, T. L. Yang, X. Z. Guo and S. R. Wang, *J. Mater. Chem.*, 2011, **21**, 349–356.
17 L. J. Wan, A. M. Cao, J. S. Hu, H. P. Liang, W. G. Song, X. L. He, X. G. Gao and S. H. Xia, *J. Phys. Chem. B*, 2006, **110**, 15858–15863.
18 X. H. Liu, J. Zhang, L. W. Wang, T. L. Yang, X. Z. Guo, S. H. Wu and S. R. Wang, *J. Mater. Chem.*, 2011, **21**, 349–356.
19 C. Z. Yuan, X. G. Zhang, L. R. Hou, L. F. Shen, D. K. Li, F. Zhang, C. G. Fan and J. M. Li, *J. Mater. Chem.*, 2010, **20**, 10809–10816.
20 H. Li, W. Li, Y. J. Zhang, T. S. Wang, B. Wang, W. Xu, L. Jiang, W. G. Song, C. Y. Shu and C. R. Wang, *J. Mater. Chem.*, 2011, **21**, 7878–7881.
21 F. Z. Mou, J. G. Guan, Z. D. Xiao, Z. G. Sun, W. D. Shi and X. A. Fan, *J. Mater. Chem.*, 2011, **21**, 5414–5421.
22 T. Sasaki, Z. P. Liu, R. Z. Ma, M. Osada, N. Iyi, Y. Ebina and K. Takada, *J. Am. Chem. Soc.*, 2006, **128**, 12162–4880.
23 L. Li, R. Ma, N. Iyi, Y. Ebina, K. Takada and T. Sasaki, *Chem. Commun.*, 2006, 3125–3127.
24 P. Gunawan and R. Xu, *Chem. Mater.*, 2009, **21**, 781–783.
25 B. Li and J. He, *J. Phys. Chem. C*, 2008, **112**, 10909–10917.
26 L. Addadi, Y. Politi, T. Arad, E. Klein and S. Weiner, *Science*, 2004, **306**, 1161–1164.
27 H. Colfen and M. Antonietti, *Angew. Chem., Int. Ed.*, 2005, **44**, 5576–5591.
28 H. J. Zhang, X. Y. Li, Z. J. Si, Y. Q. Lei, X. N. Li, J. K. Tang and S. Y. Song, *CrystEngComm*, 2011, **13**, 642–648.
29 B. Li, J. He and D. G. Evans, *Chem. Eng. J.*, 2008, **144**, 124–137.
30 L. Sun and C. Hu, *Mater. Res. Bull.*, 2011, **46**, 1922–1927.
31 B. Rebours, J. B. D. Delacaillerie and O. Clause, *J. Am. Chem. Soc.*, 1994, **116**, 1707–1717.
32 O. Clause, B. Rebours, E. Merlen, F. Trifiro and A. Vaccari, *J. Catal.*, 1992, **133**, 231–246.
33 J. H. Liu, X. Y. Yu, T. Luo, Y. X. Zhang, Y. Jia, B. J. Zhu, X. C. Fu and X. J. Huang, *ACS Appl. Mater. Interfaces*, 2011, **3**, 2585–2593.
34 Y. H. Li, F. Q. Liu, B. Xia, Q. J. Du, P. Zhang, D. C. Wang, Z. H. Wang and Y. Z. Xia, *J. Hazard. Mater.*, 2010, **177**, 876–880.
35 C. Y. Kuo and H. Y. Lin, *Desalination*, 2009, **249**, 792–796.
36 E. Alvarez-Ayuso and H. W. Nugteren, *Water Res.*, 2005, **39**, 2535–2542.
37 C. Y. Jing, M. Pena, X. G. Meng and G. P. Korfiatis, *Environ. Sci. Technol.*, 2006, **40**, 1257–1262.
38 B. Dousova, V. Machovic, D. Kolousek, F. Kovanda and V. Dornicak, *Water, Air, Soil Pollut.*, 2003, **149**, 251–267.

 